2000

Electronic Properties of Small Neutral and Charged Beryllium Clusters

Andrew M. Kolchin
Department of Physics and Astronomy, Louisiana State University, Baton Rouge

Randall W. Hall
Department of Chemistry, and Department of Physics and Astronomy, Louisiana State University, Baton Rouge, randall.hall@dominican.edu

https://doi.org/10.1063/1.1288388

Electronic properties of small neutral and charged beryllium clusters

Andrew M. Kolchin[a)]
Department of Physics and Astronomy, Louisiana State University, Baton Rouge, Louisiana 70803

Randall W. Hall[b)]
Department of Chemistry, and Department of Physics and Astronomy, Louisiana State University, Baton Rouge, Louisiana 70803

(Received 22 November 1999; accepted 16 June 2000)

We determine the atomic and electronic structures for neutral and singly positively charged beryllium clusters containing from two to six atoms using density functional theory in the local spin density approximation. Ions are moved with a steepest descent method and the electronic wave functions optimized using a fictitious dynamics with simulated annealing, as conceived by Car and Parrinello [Phys. Rev. Lett. **55**, 2471 (1985)]. Shell-like orbitals, filling angular momentum states in the order: $1s$ $1p$ $2s$ $1d$ are obtained. We employ a Mulliken population analysis using an atomic basis to examine how the shell orbitals arise from atomic orbitals. This analysis also allows us to associate the electron density distribution and, in the case of a charged cluster, the distribution of the hole with atomic sites and with regions of overlap between atom pairs. We show quantitatively that the contribution to the bonding density from delocalization of the $1s$ state is hampered by the appearance of the antibonding $2s$ state. In the case of charged clusters we observe the tendency of the hole to distribute itself near the most exterior atomic sites in geometries of high symmetry.
 [S0021-9606(00)32134-1]

I. INTRODUCTION

Clusters form a link between the atom and the bulk material. As a result, they exhibit characteristics of both forms of matter to varying degrees, depending on their size and atomic and electronic structures.[1] Much attention has been focused on clusters having magic numbers of electrons that are of unusual stability with the idea of describing them using a simplified jellium model.[2] It has been found that shell-like orbitals, delocalized over the cluster and centered at the origin of the cluster, can accurately represent the electron density in metal clusters, analogous to the electronic structure one finds in an atom. In the case of positively charged clusters, it is interesting to look at the distribution of the hole density throughout the system with a view towards identifying metallic, insulating, or intermediate behavior.

Beryllium clusters are interesting as their binding energies increase from the weakly bound dimer to a strongly bonded metal in the bulk. The drawback to beryllium is its toxicity, so that experimental data for their clusters do not exist, to our knowledge, with the exception of the dimer.[3] Beryllium clusters have been studied extensively using configuration interaction.[4–15] The results vary greatly depending on the basis sets used and beyond the five atom cluster, the use of smaller basis sets has led to some uncertainty in the nature of the lowest lying energy states.

For large clusters, density functional theory (DFT)[16,17] becomes attractive and some studies have been done using this approach. Studies of the Group IIa dimers have been made by Jones,[18] Painter and Averill,[19] and by Ortiz and Ballone.[20] Khanna, Reuse, and Buttet (KRB)[21] performed all electron calculations for neutral, singly, and doubly charged clusters of up to five atoms. Blaisten-Barojas and Khanna[22] fitted a classical many-body potential to the results, predicted the structural and binding properties for much larger clusters, and investigated the approach to the bulk material. Kawai and Weare (KW)[23] used a pseudopotential, optimized the atomic and electronic properties simultaneously, and predicted the growth and evolution of neutral Be clusters of up to 20 atoms. All of this work has been in the framework of the local spin density (LSD) approximation[16,17] with the exception of that of Ortiz and Ballone,[20] who used gradient corrections to the density in the exchange-correlation potentials.

In the present work, we study small neutral and singly positively charged clusters in the framework of DFT and LSD, describing in detail the nature of the bonding and its relationship to shell-like Kohn–Sham (KS) orbitals obtained and the relationship of these orbitals to similarly calculated atomic orbitals. For the charged clusters, we focus on the distribution of the hole density.

II. METHOD OF CALCULATION

Our studies involved neutral and singly charged Be clusters having from one to six atoms. Only the singlet or doublet states were investigated with the exception of the six atom clusters, for which spin multiplicities through the quintet were investigated. We used Perdew and Zunger's LSD[24] parametrization of the Ceperley–Alder work[25] done on the electron gas. A norm conserving pseudopotential[26] up to d nonlocality was used, with the Fourier coefficients calculated exactly in the semilocal form.

[a)]Electronic mail: kolchin@rouge.phys.lsu.edu
[b)]Electronic mail: rhall@lsu.edu

TABLE I. Convergence of binding energy per atom E_b with changes in box length L and energy cutoff E_{cut} for the neutral Be_5 cluster.

$E_{cut}=6.0$ Ry				
L (a.u.)	18	20	22	23[a]
E_b (eV/atom)	1.27	1.26	1.25	1.24
$L=20.0$ (a.u.)				
E_{cut}(Ry)	5.5	6.0	6.5	
E_b (eV/atom)	1.24	1.26	1.27	

[a]Ions fixed in the geometry obtained from the case of $L=20$ a.u.

The clusters were enclosed in a simple cubic cell of side-length 20 a.u. and the KS eigenfunctions expanded over plane waves up to an energy cutoff of 6 Ry. Convergence criteria related to these parameters are shown in Table I for the Be_5 cluster. While total energies may vary appreciably with changes in the energy cutoff, the binding energies differ much less. The geometries corresponding to the lowest energies obtained proved to be nearly identical.

The KS energy functional was minimized for both atomic and electronic structure. Ions were moved using an optimized steepest descent algorithm. Runs were performed both with and without constraints to some specific symmetry. Constrained runs were subsequently relaxed and the most stable configurations are reported here. After each move of the ions, the Fourier coefficients were reoptimized using a fictitious dynamics with simulated annealing, as conceived by Car and Parrinello.[27] We typically used a fictitious mass and initial temperature of 1 a.u. and 500 K, annealing 20 times between ion moves. The temperature was reduced by 10% at each anneal and we used the Verlet algorithm with a variable time step ranging from 5.0×10^{-3} to 2.5×10^{-4} fs, depending on stability criteria tested for periodically in the code. After each ion move, the fictitious temperature was reset to 80% of the value it had at the start of the previous optimization cycle. Convergence of the total energy was taken beyond 10^{-7} Ry, and the average distances between ions, beyond 10^{-4} a.u.

Expanding the KS orbitals over a plane wave basis and optimizing the Fourier coefficients introduces an arbitrariness into the spatial form of these orbitals, since any linear combination of such orbitals will yield the same energy. By diagonalizing the KS Hamiltonian over the basis of these orbitals, however, we arrived at shell-like orbitals for the clusters. These new orbitals, $\{\psi_i\}$, were projected on spherical harmonics located at the center of geometry of the cluster and the resulting radial distributions, $\{C^i_{lm}(r)\}$, numerically integrated for each l value to arrive at weights w^i_l for each orbital. That is,

$$C^i_{lm}(r)=\int_\Omega \psi_i(\mathbf{r})Y^*_{lm}(\Omega)d\Omega$$

and

$$w_{l_i}=\sum_m \int C^i_{lm}(r)r^2\,dr.$$

These orbitals turned out to be surprisingly pure in their dominant l components, as will be seen in Sec. III.

III. RESULTS FOR NEUTRAL CLUSTERS

The excitation energy of the Be atom from the singlet to the triplet state was calculated to be 2.67 eV, in close agreement with the experimental value of 2.73 eV.[28] This same

TABLE II. Binding energies and geometries for neutral beryllium clusters $n=1-6$.

Cluster size	Spin state	Equilibrium geometry	Binding energy/atom (eV) (bond lengths) (a.u.)			
			This work	a	b,c	d
2	singlet		0.18 (4.84)	0.18 (4.87)	0.05[e] (4.65)	
3	singlet	equilateral triangle	0.57 (4.21)	0.53 (4.33)	0.00, 0.16 (4.69)	0.31 (4.23)
4	singlet	regular tetrahedron	1.18 (3.93)	1.09 (4.04)	0.42, 0.73 (3.98)	0.90 (3.94)
5	singlet	trigonal bipyramid	1.26 (3.91 base) (3.90 apical)	1.22 (3.88 base) (4.01 apical)	0.47, 0.79 (3.86 base) (4.00 apical)	1.06 (3.84 base) (3.94 apical)
6	singlet	regular octahedron	1.21 (3.94)	1.59[f] (3.97)	⋯	0.987 distorted
6	triplet	regular octahedron[g]	1.22 (3.95)	⋯	⋯	⋯
6	quintet	regular octahedron	1.22 (3.96)	⋯	0.44, 0.82 3.94	⋯

[a]Reference 21 LSD calculations, all electron with GTO $(9s,3p)$ basis set.
[b]Reference 13 $MP4$/6-31G.
[c]Reference 13 $MP4$/6-31G^*.
[d]Reference 15 $MP4$/6-311$+G^*$ for energies of $n=3-5$, $MP4$/6-311G^* for energy of $n=6$, $MP2$/6-311$+G^*$ for bond lengths of $n=3-5$ $MP2$/6-31G^* for bond lengths of $n=6$.
[e]Reference 9.
[f]Reference 22; interatomic potential fit to Ref. 21.
[g]Slightly distorted; bond lengths ranging from 3.94 to 3.95 a.u.

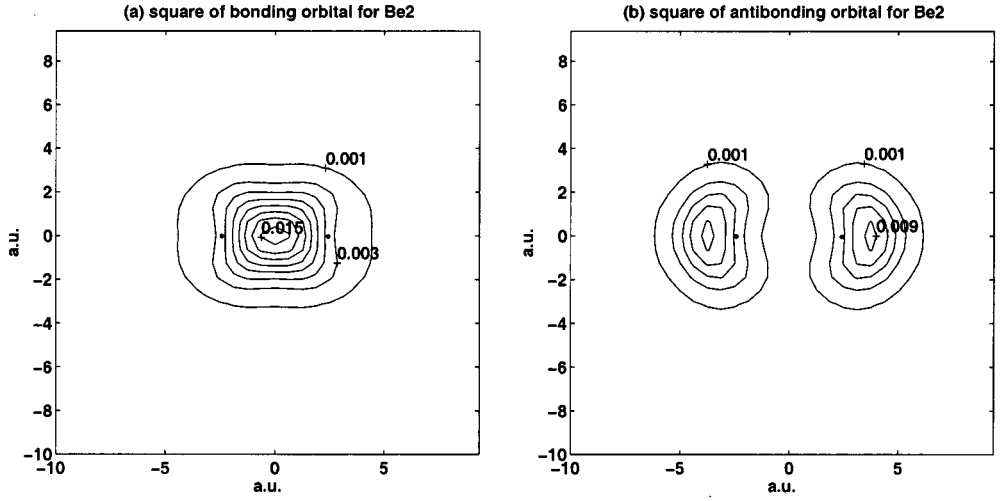

FIG. 1. Contours in a plane through the atoms, of the squares of singly occupied bonding and antibonding orbitals for Be_2. Filled circles indicate projected positions of the ions. Units are electrons/a.u.

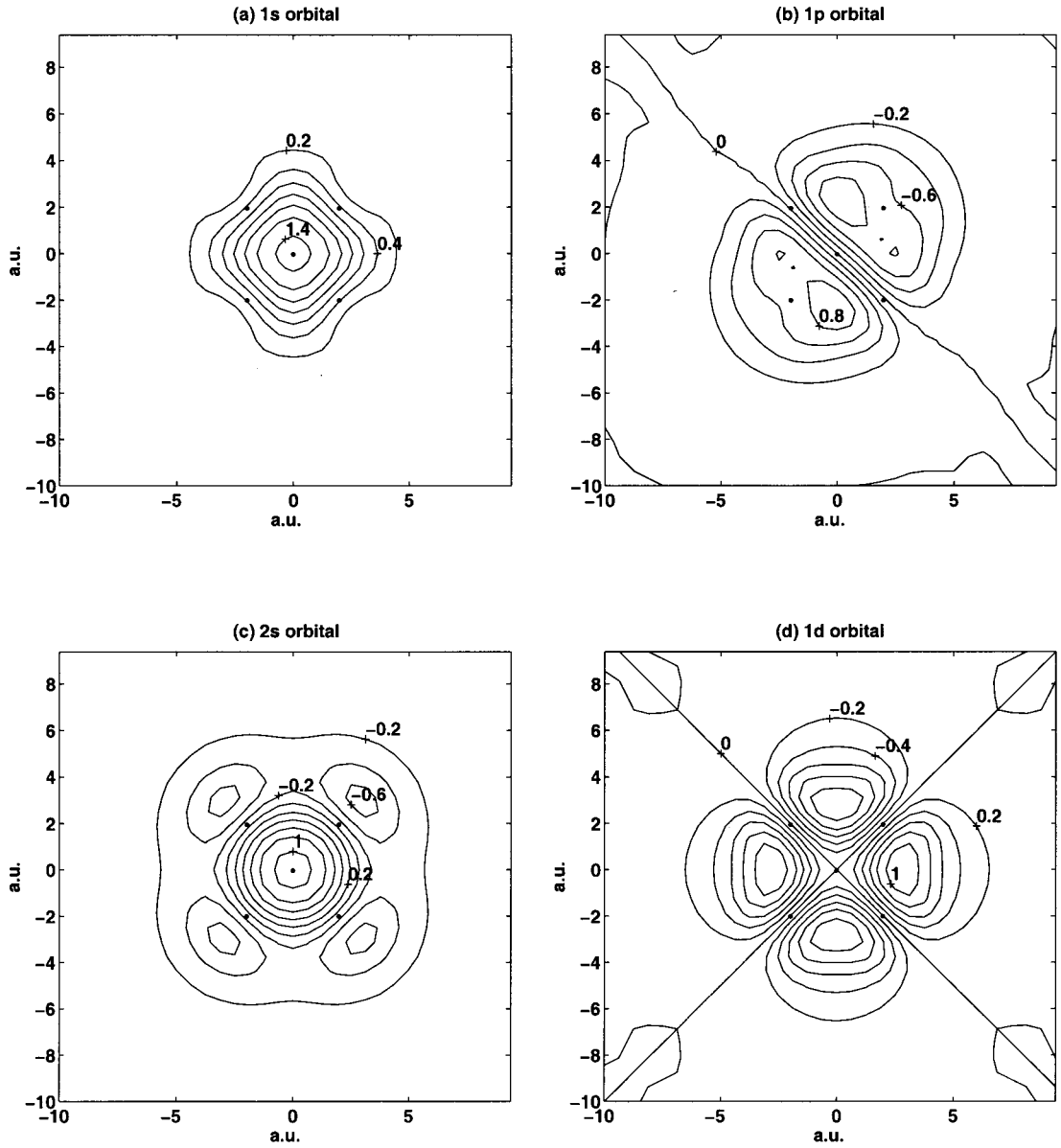

FIG. 2. Contours in a plane containing four atoms of the octahedron of some orbitals of the Be_6 quintet. Filled circles indicate projected positions of ions. Units are in 10^{-3}/a.u.

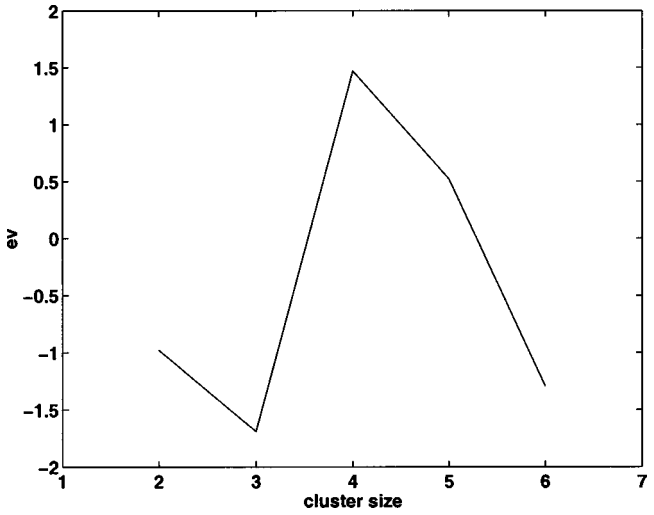

FIG. 3. Second difference of the energy: $\Delta_2(N)=E(N+1)+E(N-1)-2E(N)$ plotted against cluster size N. The point at $N=6$ is calculated from the lowest energy we have currently obtained for the seven atom cluster, a singlet centered hexagon.

calculated value was obtained whether by taking the difference of the energies of the two states or by taking the difference of their highest lying KS eigenvalues. The latter calculation suggests that while the KS eigenvalue of the highest occupied state, calculated using LSD, may fall short of its theoretical correspondence to the first ionization potential[29,30] (our 5.41 eV compared to the experimental 9.32 eV),[28] differences in eigenvalues may be more useful. This is consistent with recent work done by Stowasser and Hoffmann,[31] who propose a linear scaling be applied to eigenvalues for quantitative interpretation.

The geometries and binding energies of our lowest energy configurations are shown in Table II for clusters containing up to six atoms, along with the results of earlier calculations. The binding energies are slightly higher than those obtained by KRB, whose all electron LSD calculations used a Gaussian type orbital (GTO) $(9s,3p)$ basis set, and lower than those of KW, whose calculations, while similar to ours, used larger energy cutoffs with the Kleinman–Bylander transformation.[32]

The dimer is the only cluster, to our knowledge, for which experimental data exist. Bondeybey,[3] using laser induced fluorescence, measured a binding energy of 0.10 eV and a separation of 4.63 a.u. for the $X\,^1\Sigma_g^+$ ground state. Specific results of CI calculations for the dimer are reviewed extensively by Harrison and Handy.[9] Their own values of 0.098 eV and 4.65 a.u. are very close to the experimental result. Our values of 0.36 eV with a separation of 4.84 a.u. are typical of LSD calculations, comparing well with the all-electron results of KRB who obtained the same binding energy with a slightly higher bond length of 4.87 a.u. Significantly higher binding energies were calculated by Painter and Averill[19] using LSD with other exchange-correlation functionals than that of Perdew and Zunger,[24] including the $X\alpha$ method, but they obtained separations very close to the experimental value.

Despite the high binding energy calculated using the LSD approximation relative to the experimental result, the KS orbitals found for the dimer were confirmed to be symmetric and antisymmetric combinations of the orbital obtained from one-atom calculations translated to the atomic sites of the dimer. The charge density due to each of these molecular orbitals is shown in Fig. 1 for the up spins, illustrating their bonding and antibonding natures. Results for the down spins are correspondingly similar. Projection of these KS orbitals onto spherical harmonics centered at the center of geometry, with the subsequent radial integration of each projection, shows the lower and higher orbitals to be almost purely s and p, respectively, in nature.

Such shell-like orbitals were obtained for clusters of up to six atoms, filling in the order of $1s\ 1p\ 2s\ 1d$. Representative orbitals are shown in Fig. 2 for the Be_6 quintet. Diagonalization of this cluster's Hamiltonian in Fourier space allowed us to see the higher unoccupied states and showed $2l+1$ orbitals for each value of l. In analogy to shell closings in atoms such as the inert gases being due to the relatively large gap between the unoccupied s state and the filled p state below it, a common measure of a cluster's stability is its second difference of the energy.[2] This is the difference between the energy gaps to the next larger cluster (or equivalently, the next state occupied by the additional electrons) and the preceding smaller cluster, that is,

$$\Delta_2(N)=[E(N+1)-E(N)]-[E(N)-E(N-1)].$$

A plot of the second difference of the energy for the neutral clusters (Fig. 3) shows a high stability for the Be_4 cluster, corresponding to a hypothetical shell closing. The fragmentation channels for the clusters are shown in Table III where we can see that all of the clusters would be most likely to

TABLE III. Fragmentation channels for neutral Be_n clusters. Energies are in eV.

$Be_{n+m}\rightarrow Be_n+Be_m$	$E_n+E_m-E_{n+m}$
$Be_6\rightarrow Be_5+Be_1$	1.04
$\rightarrow Be_4+Be_2$	2.24
$\rightarrow Be_3+Be_3$	3.93
$Be_5\rightarrow Be_4+Be_1$	1.56
$\rightarrow Be_3+Be_2$	4.22
$Be_4\rightarrow Be_3+Be_1$	3.03
$\rightarrow Be_2+Be_2$	4.00
$Be_3\rightarrow Be_2+Be_1$	1.34
$Be_2\rightarrow Be_1+Be_1$	0.36

TABLE IV. Fractional S, P, and OV populations for each cluster.

Cluster size	Spin state	S	P	OV
2	singlet	0.83	0.06	0.11
3	singlet	0.69	0.11	0.20
4	singlet	0.72	0.16	0.12
5	singlet	0.75	0.27	−0.03
6	singlet	0.51	0.36	0.14
6	triplet	0.49	0.35	0.16
6	quintet	0.45	0.36	0.20

TABLE V. Fractional *S*, *P*, and OV populations by KS orbital for neutral Be clusters.

Cluster	ψ_i[a]	Γ[b]	ϵ_i (eV)	w_{l_i}[c]	*S*	*P*	OV
Be_2	ψ_1	σ_g^+	−6.76	0.97*s*	0.58	0.04	0.38
($D_{\infty h}$)	ψ_2	σ_u^+	−4.29	0.96*p*	1.08	0.07	−0.15
Be_3	ψ_1	a_1'	−8.53	0.99*s*	0.28	0.10	0.62
(D_{3h})	ψ_2	e'	−4.56	0.96*p*	0.89	0.12	−0.01
	ψ_3	e'	−4.55	0.96*p*	0.89	0.12	−0.01
Be_4	ψ_1	a_1	−9.79	0.99*s*	0.13	0.16	0.71
(T_d)	ψ_2	t_2	−4.96	0.97*p*	0.92	0.16	−0.08
	ψ_3	t_2	−4.96	0.97*p*	0.91	0.16	−0.07
	ψ_4	t_2	−4.95	0.97*p*	0.91	0.16	−0.07
Be_5	ψ_1	a_1'	−10.91	0.98*s*	0.10	0.15	0.74
(D_{3h})	ψ_2	a_2''	−7.20	0.98p_z	0.72	0.23	0.05
	ψ_3	e'	−5.74	0.95p_y	1.09	0.18	−0.27
	ψ_4	e'	−5.74	0.95p_x	1.09	0.17	−0.26
	ψ_5	a_1'	−3.96	0.82*s*,0.12*d*	0.79	0.63	−0.41
Be_6	ψ_1	a_{1g}	−11.25	0.99*s*	0.08	0.13	0.79
(O_h)	ψ_2	t_{1u}	−6.75	0.97*p*	0.80	0.19	0.01
	ψ_3	t_{1u}	−6.73	0.97*p*	0.78	0.18	0.05
	ψ_4	t_{1u}	−6.73	0.97*p*	0.78	0.18	0.05
	ψ_5	a_{1g}	−4.07	0.96*s*	0.54	0.66	−0.20
	ψ_6	t_{2g}	−3.49	0.98*d*	0.00	0.74	0.26
	ψ_7	t_{2g}	−3.48	0.98*d*	0.00	0.78	0.22
	ψ_8	t_{2g}	−3.48	0.98*d*	0.00	0.78	0.22
	$\psi_{1\downarrow}$	a_{1g}	−10.42	0.99*s*	0.07	0.14	0.79
	$\psi_{2\downarrow}$	t_{1u}	−5.82	0.97*p*	0.77	0.18	0.05
	$\psi_{3\downarrow}$	t_{1u}	−5.80	0.97*p*	0.75	0.17	0.09
	$\psi_{4\downarrow}$	t_{1u}	−5.80	0.97*p*	0.75	0.17	0.09

[a]Orbitals are spin up unless otherwise noted. For singlet states of two through five atoms, spin down figures are very nearly the same. All orbitals are shown for the Be_6 quintet.
[b]Irreducible representations.
[c]Components amounting to less than 5% are omitted.

fragment into the next smallest cluster with the loss of one atom. The high dissociation energy for the Be_4 cluster indicates once again, its high stability.

The symmetries of our lowest energy clusters agree with those of KRB for beryllium, and to similar work done by Reuse, Khanna, deCoulon, and Buttet (RKCB)[33] on magnesium for clusters containing up to five atoms. For the six atom cluster, our binding energies and geometries came out very nearly the same for all the spin multiplicities investigated. While our result agrees well geometrically with the CI calculations of Marino and Ermler[13] for the Be_6 quintet (their ground state), they obtain trigonal antiprisms for the less stable singlet and triplet states. A distorted singlet structure of C_{2v} symmetry (a trapezoidal bipyramid) has been reported by Sudhakar and Lammertsma (SL) which they attribute to the Jahn–Teller effect.[34] The orbitals obtained by us for the Be_6 quintet (an undistorted octahedron) form a spatially nondegenerate system with complete fillings of the $1s$, $1p$ shells (two electrons per orbital) and the $2s$ and $1d$ shells (one electron per orbital), the latter being triply degenerate (t_{2g}), leaving the doubly degenerate (e_g) *d* shell completely unoccupied. We obtained a slightly distorted octahedron for the triplet state with two nondegenerate *d* orbitals; a

TABLE VI. Convergence of binding energy E_b with changes in box length L for the charged Be_5^+ cluster.

$E_{cut}=6.0\,Ry$				
L (a.u.)	18	20	22	23[a]
E_b[b] (eV)	8.94	8.81	8.74	8.73
E_b[c] (eV)	8.60	8.57	8.56	8.57

[a]Ions fixed in the geometry obtained from the case of $L=20$ a.u.
[b]Uncorrected.
[c]Corrected according to Ref. 39.

TABLE VII. Binding energies and geometries for charged beryllium clusters $n=1-6$.

			Binding energy (eV) (Bond lengths) (a.u.)	
Cluster size	Spin state	Equilibrium geometry	This work a,b	KRB c
2	doublet	⋯	2.18, 2.22 (4.24)	2.19 (4.33)
3	doublet	linear	3.85, 3.91 (4.17)	3.91 (4.23)
4	doublet	distorted tetrahedron	5.79, 5.96 (4.12 average)	5.61 (3.90, 4.43)
5	doublet	trigonal bipyramid	8.57, 8.80 (4.08 base) (3.99 apical)	8.45 (4.02 base) (4.08 apical)
6	doublet	regular octahedron	9.58, 9.90 (4.00)	—
6	quartet	regular octahedron	9.69, 9.99 (4.02)	—

[a]Corrected using Ref. 39.
[b]Uncorrected.
[c]Reference 21 LSD calculation.

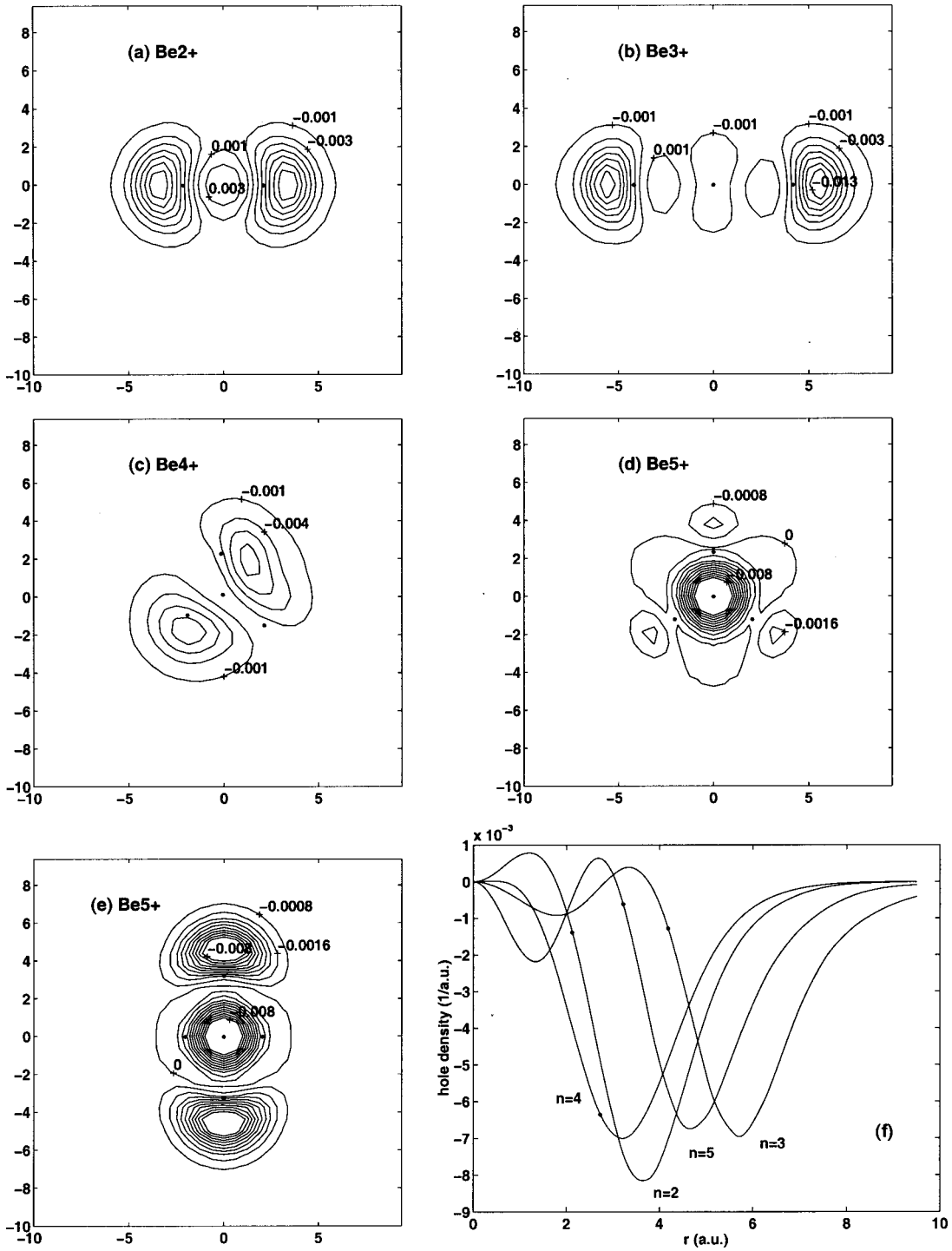

FIG. 4. (a)–(d) Contours in the equatorial plane of the hole density: $n_{\downarrow}(\mathbf{r})-n_{\uparrow}(\mathbf{r})$. Filled circles indicate projected positions of ions. (e) Same for Be_5^+ in a plane perpendicular to the trigonal base. (f) Radial distributions of the hole density for clusters of two through five atoms. Filled circles indicate positions of atoms furthest from the origin. Units are electrons/a.u.

mostly $d_{x^2-y^2}$ orbital lying 0.16 eV below an orbital containing nearly equal mixtures of the *xy*, *xz*, and *yz* bases, the octahedral symmetry being sufficiently violated to break the t_{2g}/e_g degeneracies. The distortion was obtained by relaxing a constraint to octahedral symmetry with a reheat of the electronic degrees of freedom, resulting in a lowering of the energy by 0.10 eV. Our lowest energy singlet state turned out to be an undistorted octahedron despite our expectations of obtaining a Jahn–Teller distorted structure. Two singly occupied *d* orbitals of opposite spin were obtained; a d_{xz} and a d_{yz}. Reheating of this cluster with a subsequent relaxing of the octahedral constraint, and investigation using constraints to the lower symmetries of rectangular and rhombus based bipyramids, SL's C_{2v} structure, and the trigonal antiprism did not yield lower energies. For the analogous Mg_6 cluster RKCB report a singlet rectangular bipyramid as their ground state. Our inability to obtain the expected distortion is probably due to the breaking of octahedral symmetry for the

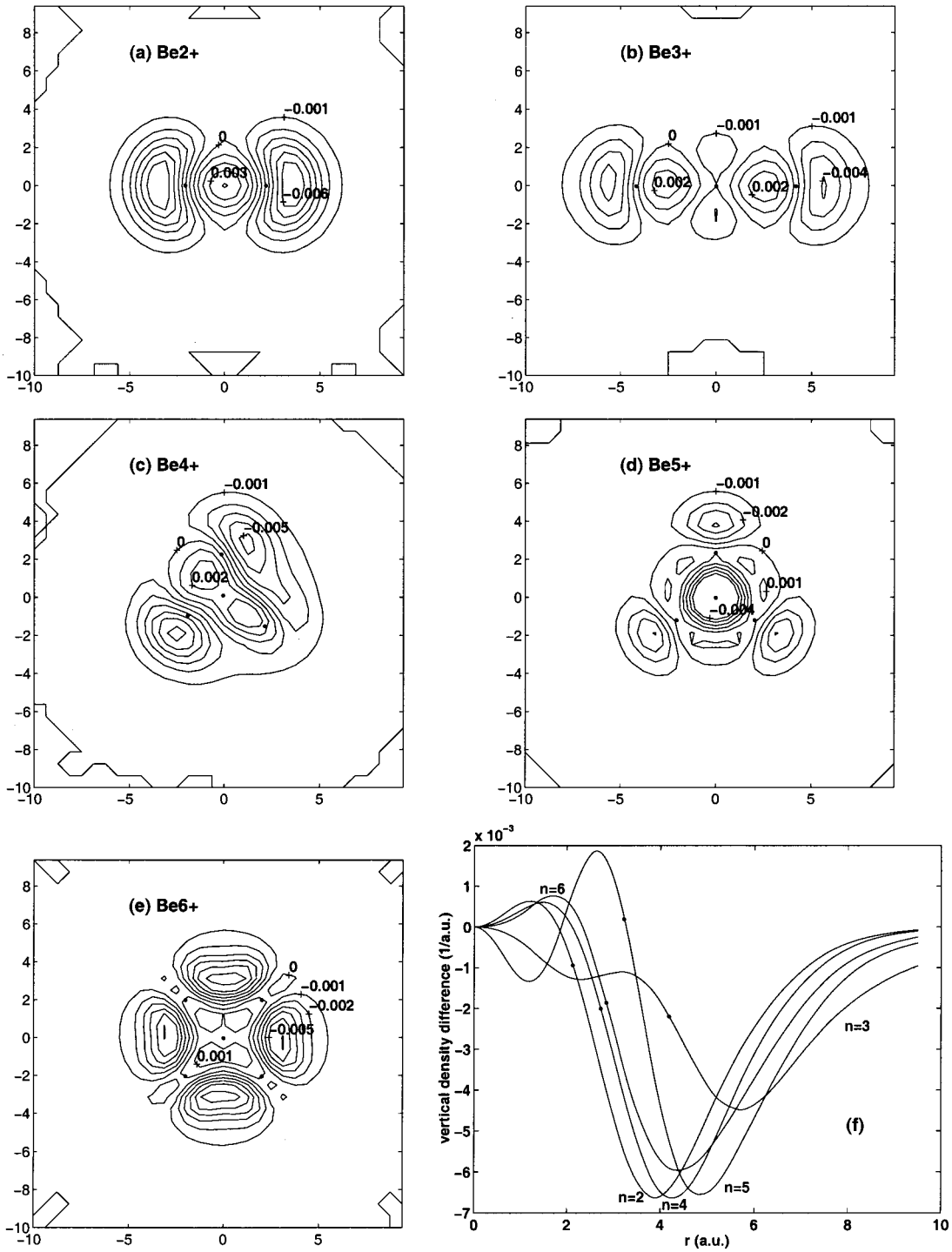

FIG. 5. (a)–(e) Contours in the equatorial plane of the vertical density difference. Circles indicate projected positions of the ions. (f) Radial distributions of the hole density for clusters of two through five atoms. Filled circles indicate positions of atoms furthest from the origin. Units are electrons/a.u.

overall system of the cluster and its periodic images by using the supercell method along with our use of singly occupied orbitals (a standard approach to DFT–LSD calculations). The latter leads to a breaking of symmetry with even small differences in distributions between the up/down orbital pairs. This feature of DFT calculations has been recognized and corrections proposed[35] but we have not included them in the present work. Our focus here is on how atomic orbitals may hybridize to form shell-like KS orbitals and we do not expect the trends in our results to be significantly changed by an analysis of the correct Jahn–Teller distorted structures.

By diagonalizing the Hamiltonian after optimization for one atom in Fourier space we obtained the four lowest lying (one occupied *s* and three virtual *p*) atomic orbitals. These were used to form an atomic basis $\{|\phi_i\rangle\}$ for each cluster, composed of copies of these orbitals translated to the atomic

TABLE VIII. Distribution of the hole density at atomic sites and in overlap regions. Lower off diagonal elements have been incorporated into the upper off diagonal elements. Negative numbers refer to higher concentrations of the hole. Refer to Fig. 6 for the geometry and numbering of the atoms.

	Be_2^+				
	1	2			
1	−0.65	0.31			
2	—	−0.64			
		Be_3^+			
	1	2	3		
1	−0.50	0.13	−0.04		
2	—	−0.19	0.14		
3	—	—	−0.52		
		Be_4^+			
	1	2	3	4	
1	−0.60	0.76	−0.34	0.11	
2	—	−0.71	0.21	−0.30	
3	—	—	−0.09	0.07	
4	—	—	—	−0.07	
		Be_5^+			
	1	2	3	4	5
1	−0.09	−0.03	−0.03	0.09	0.09
2	—	−0.09	−0.03	0.09	0.09
3	—	—	−0.10	0.10	0.10
4	—	—	—	−0.57	−0.03
5	—	—	—	—	−0.57

sites. Each KS orbital (KSO), $|\psi_i\rangle$ was then expanded over this basis as $|\psi_i\rangle=\Sigma_j c_j^{(i)}|\phi_j\rangle$ and the coefficients $c_j^{(i)}$ solved for, in order to see how such orbitals might arise as linear combinations of atomic orbitals. This also allows us to perform a Mulliken population analysis[36] by constructing a matrix from the terms that sum to form the inner product of each KSO as

$$\langle\psi_i|\psi_i\rangle=1\approx\sum_j q_j^{(i)}+\sum_j\sum_{k>j} p_{jk}^{(i)}$$

with

$$q_j^{(i)}=|c_j^{(i)}|^2$$

and

$$p_{jk}^{(i)}=2\,\mathrm{Re}(c_j^{(i)*}c_k^{(i)}\langle\phi_j|\phi_k\rangle),$$

where the lower diagonal elements have been incorporated into those of the upper diagonal.

The diagonal elements $\{q_j^{(i)}\}$ give a measure of each KS orbital's contribution to density populations associated with atomic sites, while the off diagonal elements $\{p_{jk}^{(i)}\}$ reflect contributions to density populations associated with regions of overlap (OV) between pairs of atoms. Positive, negative, and small OV populations typically indicate bonding, antibonding, and nonbonding regions, respectively.[37] The elements of the matrix sum very nearly to unity for each orbital, showing that only *sp* hybridization occurs.

We can sum the *p*-type contributions at each atomic site to determine the *s*-type and *p*-type populations at these sites. Further, we can sum all contributions at each atomic site and in each overlap region to give the overall contribution to the

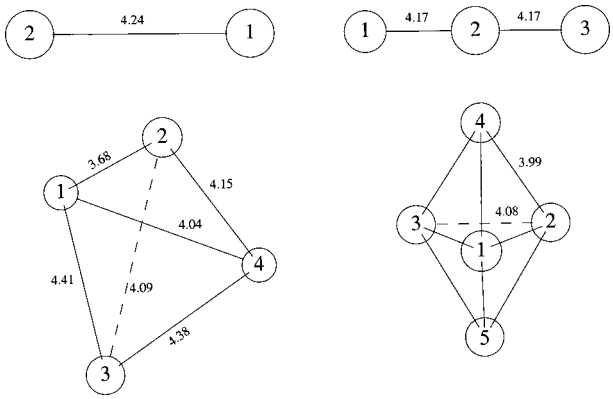

FIG. 6. Geometries and numbering of atoms in charged clusters. Distances are in a.u.

electron density at each site due to a KSO. Summing such contributions over all KSOs then gives us the total electron density for each atomic site and overlap region due to all electrons in the cluster. Table IV shows the total *s* and *p* fractional populations associated with atomic sites (*S* and *P*) and the total OV fractional population in each cluster. From this, we can see an overall decrease in *s* and increase in *p* populations with increasing cluster size. A dramatic decrease in the OV population occurs at the five atom cluster due to the advent of a $2s$ orbital, whose contribution to the OV population is -0.41 electrons per orbital. In general, the higher lying KSOs are more localized on atomic sites. Increases in the OV population with the addition of atoms to a cluster appear to arise mainly from further delocalization of the lowest lying state. This situation is clearly shown in Table V which shows the breakdown of these contributions by the KSOs along with their KS eigenvalues for each cluster. The six atom cluster is particularly interesting as it shows shell-like *p* orbitals to be composed mainly of localized, atomic *s* orbitals and shell-like *d* orbitals to be composed mainly of localized, atomic *p* orbitals. As noted above, the $1s$ orbital arises from atom-pair overlaps, while the $2s$ orbital, in stark contrast, arises from *sp* hybridization localized at the atomic sites.

IV. RESULTS FOR CHARGED CLUSTERS

Our treatment of the charged clusters is based on the artificial introduction of a neutralizing uniform charge density into the supercell, as suggested by Leslie and Gillian, [38] in order to maintain the cancellation of singularities arising from contributions at the origin of the Fourier space to the potentials. This background jellium tends to zero in the limit of large supercells. Usage of the Makov–Payne correction[39] allows us to subtract out some of the nonphysical effects due to the jellium and due to the interactions between clusters arising from the use of periodic boundary conditions. These corrections are taken through the order of $1/L^3$, where L is the box length of a simple cubic cell. In Makov and Payne's treatment, superimposed positive and negative point charges, equal in magnitude to the cell's net charge, are added to the system to allow separation of the total charge density into two separate neutral densities: one containing the jellium and

one the calculated density. Placement of these charges is chosen to render the latter term's dipole moment to be zero. These corrections were used to adjust our final energies, but were omitted from our fictitious dynamics. Our estimate of the ionization energy for the Be atom, calculated as the difference in energies between the charged and the neutral species, rose from 6.87 to 8.85 eV as compared with the experimental value of 9.32 eV.[28] The major portion of this rise (>97.5%) is due to the interaction of the jellium with the monopole moment (net charge) of the cluster. The rest is proportional to the quadrupole moment of the calculated charge distribution with the embedded point charge. The first term, being independent of cluster size, subtracts out in the calculation of binding energies. The latter term was found to have a dramatic effect in lowering the binding energies obtained and in converging our energies with box length. This is evident from Table VI, which compares corrected and uncorrected binding energies obtained for the Be_5^+ cluster at various box lengths. As with the neutral clusters, the geometries corresponding to the lowest energies were nearly independent of box length.

Table VII shows the most stable geometries of the charged clusters along with their binding energies. The binding energy of a cluster of n atoms was calculated as

$$E_b(n)=E_{\mathrm{Be}_n^+}-((n-1)E_{\mathrm{Be}_1}+E_{\mathrm{Be}_1^+}).$$

The removal of an electron from the three atom cluster resulted in a symmetric linear arrangement lower in energy from the undistorted C_{3v} symmetry by 0.36 eV, consistent with the work of KRB on beryllium and with that of RKCB, Eriksson,[40] Davidson and Frey(DF),[41] and Knight *et al.*[42] on magnesium; the latter using self-consistent field with correlation effects taken into account. We obtained a highly distorted tetrahedron for the four atom cluster, consistent with the work of KRB, and in contrast to their (RKCB), Eriksson's, and DF's similar work on magnesium in which slightly lower lying linear arrangements were found. The large extent of the linear cluster renders its investigation impractical in the present work due to the surface effects inherent in the supercell method. For the five atom cluster we obtained an undistorted trigonal biprism as did KRB for beryllium and RKCB, Eriksson, and DF for magnesium. For the case of Be_6^+ we investigated starting configurations of the octahedron and the rectangular bipyramid with runs constrained to these symmetries (with a subsequent reheat and relaxation of the constraints) along with unconstrained runs. The clusters of O_h symmetry yielded the lowest energies in contrast to the work of RKCB on magnesium, who arrived at the rectangular bipyramid as their lowest energy configuration. Eriksson reported a triangular biprism as lying 0.35 eV below the rectangular bipyramid for Mg_6^+, while DF found a trapezoidal bipyramid to lie 0.25 eV below rhomboidal and rectangular bipyramids. The latter two configurations were found to be nearly degenerate with the rectangular bipyramid lying about 3 meV higher than the rhomboidal bipyramid. We found the geometries of the doublet and quartet states of Be_6^+ to be similar with the former having a bond length shorter by 0.02 a.u. and an energy greater by about 0.11 eV. Again, our more symmetric structures are probably due to symmetry-breaking issues discussed above for the neutral clusters, the problem of periodic boundary conditions being much more pronounced for charged clusters.

Our interest centers on the distribution of the hole density. One spin down electron was removed to create the hole. In the course of our calculations on the doublet clusters, we have found every spin down electron to pair with a spin up electron to the extent that the projection of one's orbital onto the other is within 0.01 of unity, with the exception of the Be_4^+ cluster which has one pair projection of 0.98 and another of 0.90. The spin density: $n_\downarrow(\mathbf{r})-n_\uparrow(\mathbf{r})$ can therefore be taken as a good measure of the hole density for the doublet clusters $n=2$ through $n=5$. Following the example of KRB, we also calculated the difference in electron density between charged clusters and neutral clusters having the charged geometry. For convenience, we denote this as the vertical density difference. Figures 4 and 5 show contours of the hole density and the vertical density difference, respectively, along with their radial distributions. The position of the outermost atom from the origin is marked on each curve. Since negative values correspond to regions of higher hole density, we can see from the contour plots that the hole is mostly distributed outside the cluster in all cases. An interesting trapping of a small portion of the hole within the base of the trigonal bipyramid is found in Be_5^+.

To get some quantitative measure of the distribution of the hole density, we summed the Mulliken population matrices for the down spins and the up spins and took the difference between these two matrices. Where negative numbers refer to regions of abundant hole density, Table VIII shows the distribution of the hole relative to atomic positions and to overlap regions between atoms. Refer to Fig. 6 for the geometry and numbering of the atoms used in Table VIII. Inspection of the distributions shows the tendency of the hole to distribute itself at the extreme ends of the cluster, accompanied by a smaller tendency to lie in the vicinity of atomic sites. This is especially noticeable for the three and five atom clusters.

The asymmetric four atom cluster has two atoms, labeled 1 and 2 in Fig. 6, that are particularly close to each other. These atoms trap a large percentage of the hole in a way that is very similar to the case of the charged dimer. Each of the two other atoms attracts some of the hole density from one of the first two atoms, causing an appreciable delocalization into the overlap regions between two pairs of atoms (atoms 1 and 3; atoms 2 and 4 in Fig. 6).

V. CONCLUSIONS

In this work, we have shown how small beryllium clusters have characteristics typical of a shell model from the points of view of stability and electronic structure. We found a higher relative stability for the four atom cluster with the magic number of eight valence electrons and obtained orbitals of mostly pure l states centered about each cluster's center of geometry. These orbitals were expanded over a similarly calculated atomic basis to see how they might arise from hybridization of atomic orbitals and to examine how they contribute to the overall binding in the cluster. An

atomic basis consisting solely of s and p orbitals was found to be very nearly complete in describing the shell-like orbitals. We identified the order of filling for the l states, namely, $1s1p2s1d$. Further, using a Mulliken population analysis, we found the $1s$ state to be highly delocalized, the $2s$ state to be highly localized and hybridized, and the $1p$ and $1d$ states to be localized and composed mainly of pure s and pure p atomic orbitals, respectively.

In a similar fashion, we decomposed the hole densities for the singly positively charged clusters into contributions to the population density in regions of atomic sites and in regions of overlap between pairs of atoms. We showed the hole's tendency to be concentrated at the extreme extents of the cluster and, in clusters of high symmetry, to favor atomic sites rather than overlap regions.

ACKNOWLEDGMENTS

We are grateful to the Louisiana State University Board of Regents and to the National Science Foundation for funding the major part of this work. We also thank the Concurrent Computing Laboratory for Material Simulations, the Computer Science Department, and the Office of Computing Services, all at Louisiana State University, for providing the computing facilities used in our calculations.

[1] A. W. Castleman, Jr. and K. H. Bowen, Jr., J. Phys. Chem. **100**, 12911 (1996).
[2] W. A. deHeer, W. D. Knight, M. Y. Chou, and M. L. Cohen, Solid State Phys. **40**, 93 (1987).
[3] V. E. Bondybey, Chem. Phys. Lett. **109**, 436 (1984).
[4] R. A. Whiteside, R. Krishnan, J. A. Pople, M. Krogh-Jespersen, P. von Rague Schleyer, and G. Wenke, J. Comput. Chem. **1**, 307 (1980).
[5] G. Pacchioni and J. Koutecky, Chem. Phys. **71**, 181 (1982).
[6] C. W. Bauschlicher, Jr., P. S. Bagus, and B. N. Cox, J. Chem. Phys. **77**, 4032 (1982).
[7] B. H. Lengsfield III, A. D. McLean, M. Yoshimine, and B. Liu, J. Chem. Phys. **79**, 1891 (1983).
[8] G. Pacchioni, W. Pewestorf, and J. Koutecky, Chem. Phys. **83**, 261 (1984).
[9] R. J. Harrison and N. C. Handy, Chem. Phys. Lett. **123**, 321 (1986).
[10] W. C. Ermler, C. W. Kern, R. M. Pitzer, and N. W. Winter, J. Chem. Phys. **84**, 3937 (1986).
[11] C. W. Bauschlicher and L. G. M. Pettersson, J. Chem. Phys. **84**, 2226 (1986).
[12] C. M. Rohlfing and J. S. Binkley, Chem. Phys. Lett. **134**, 110 (1986).
[13] M. M. Marino and W. C. Ermler, J. Chem. Phys. **86**, 6283 (1987).
[14] T. J. Lee, A. P. Rendell, and P. R. Taylor, J. Chem. Phys. **92**, 489 (1989).
[15] P. V. Sudhakar and K. Lammertsma, J. Chem. Phys. **99**, 7929 (1993).
[16] P. Hohenberg and W. Kohn, Phys. Rev. **136**, B864 (1964).
[17] W. Kohn and L. J. Sham, Phys. Rev. **140**, A1133 (1965).
[18] R. O. Jones, J. Chem. Phys. **71**, 1300 (1979).
[19] G. S. Painter and F. W. Averill, Phys. Rev. B **26**, 1781 (1982).
[20] G. Ortiz and P. Ballone, Z. Phys. D: At., Mol. Clusters **19**, 169 (1991).
[21] S. N. Khanna, F. Reuse, and J. Buttet, Phys. Rev. Lett. **61**, 535 (1988).
[22] E. Blaisten-Barojas and S. N. Khanna, Phys. Rev. Lett. **61**, 1477 (1988).
[23] R. Kawai and J. H. Weare, Phys. Rev. Lett. **65**, 80 (1990).
[24] J. P. Perdew and A. Zunger, Phys. Rev. B **23**, 5048 (1981).
[25] D. M. Ceperley and B. J. Alder, Phys. Rev. Lett. **45**, 566 (1980).
[26] G. B. Bachelet, D. R. Hamann, and M. Schluter, Phys. Rev. B **26**, 4199 (1982).
[27] R. Car and M. Parrinello, Phys. Rev. Lett. **55**, 2471 (1985).
[28] J. Emsley, *The Elements*, 2nd ed. (Clarendon, Oxford, 1991).
[29] J. P. Perdew, R. G. Parr, M. Levy, and J. L. Balduz, Jr., Phys. Rev. Lett. **49**, 1691 (1982).
[30] C. O. Almbladh and U. von Barth, Phys. Rev. B **31**, 3231 (1985).
[31] R. Stowasser and R. Hoffmann, J. Am. Chem. Soc. **121**, 3414 (1999).
[32] L. Kleinman and D. M. Bylander, Phys. Rev. Lett. **48**, 1425 (1982).
[33] F. Reuse, S. N. Khanna, V. de Coulon, and J. Buttet, Phys. Rev. B **41**, 11743 (1990).
[34] H. A. Jahn and E. Teller, Proc. R. Soc. London, Ser. A **161**, 220 (1937).
[35] J. Grafenstein, E. Kraka, and D. Cremer, Chem. Phys. Lett. **288**, 593 (1998).
[36] R. S. Mulliken, J. Chem. Phys. **23**, 1833 (1955); **23**, 1841 (1995); **23**, 2338 (1995); **23**, 2343 (1955).
[37] I. N. Levine, *Quantum Chemistry*, 5th ed. (Prentice Hall, Englewood Cliffs, NJ, 2000), p. 506.
[38] M. Leslie and M. J. Gillan, J. Phys. C **18**, 973 (1985).
[39] G. Makov and M. C. Payne, Phys. Rev. B **51**, 4014 (1995).
[40] L. A. Eriksson, J. Chem. Phys. **103**, 1050 (1995).
[41] E. R. Davidson and R. Frey, J. Chem. Phys. **106**, 2331 (1997).
[42] L. B. Knight, C. B. Cleveland, R. F. Frey, and E. R. Davidson, J. Chem. Phys. **100**, 7867 (1994).